Changes in Secondary Structure and Salt Links of Cytochrome P-450$_{cam}$ Induced by Photoreduction: A Fourier Transform Infrared Spectroscopic Study†

Jörg Contzen and Christiane Jung*

Max-Delbrück-Centrum für Molekulare Medizin, Robert-Rössle-Strasse 10, D-13092 Berlin, Germany

Received July 28, 1999; Revised Manuscript Received September 28, 1999

ABSTRACT: Tris(2,2′-bipyridyl)ruthenium(II) was used as a light-induced artificial electron donor for the transfer of the first electron to cytochrome P-450$_{cam}$ bound with (1*R*)-camphor and camphane substrates, and in the substrate-free form. Fourier transform infrared spectroscopy was used to detect changes of the amide I′ band and the CO ligand stretch vibration of heme-bound carbon monoxide associated with the heme redox transition. The reduced-minus-oxidized difference spectra show that not only the heme group but also the protein backbone and individual amino acid side chains were affected by the redox transition. Observed secondary structure changes were almost identical for (1*R*)-camphor-bound and camphane-bound cytochrome P-450$_{cam}$, with a remarkable negative signal at 1724.3 cm^{-1} and a positive signal at 1716.0 cm^{-1}. These signals were not observed in substrate-free P-450$_{cam}$. On the basis of known crystallographic data, we assign these signals to a change of hydrogen bonds of a salt link between Arg112, His355, and the heme 6-propionic group.

Enzymes of the cytochrome P-450[1] superfamily are heme protein monooxygenases that catalyze the hydroxylation of various substrates in many organisms. Their unique ability to cleave the bond of molecular dioxygen and hydroxylate nonactivated C−H bonds in a regio- and stereospecific manner makes them potential candidates for applications such as detoxification of environmental pollutants and biotechnological drug production (*1*−*3*).

The soluble cytochrome P-450$_{cam}$ from the soil bacterium *Pseudomonas putida* catalyzes the first step in the metabolism of (1*R*)-camphor, a monoterpene which is the sole source of carbon and energy. It hydroxylates (1*R*)-camphor to 5-*exo*-hydroxycamphor (*4*). The monooxygenase reaction requires two reducing equivalents, which are delivered from NADH to a specific transportation system composed of putidaredoxin reductase, a flavoprotein, and putidaredoxin (Pdx), an iron−sulfur protein containing an Fe_2S_2 cluster. Pdx is the direct electron donor to P-450$_{cam}$. The two electrons are transferred from reduced putidaredoxin to P-450 in two single electron transfer steps, the first reducing the heme iron from the ferric to the ferrous state and enabling subsequent binding of molecular oxygen at the sixth ligand position of the iron, and the second reducing the oxy−P-450 complex (*5*). A 7-fold lower Michaelis constant of P-450$_{cam}$ for the redox reaction with Pdx for the first electron transfer step compared to the second one and different sensitivity to ionic strength of the individual electron transfer steps led to the supposition that both steps differ fundamentally in their affinity, mechanism, or transfer path (*5*). This view is further supported by the finding that there are several competent electron donors, like spinach ferredoxin, adrenodoxin, or dithionite, that can replace putidaredoxin in the first transfer step, but not in the second one, although these artificial donors have a more negative redox potential than putidaredoxin.

In their recently published paper, Roitberg and co-workers suggest that binding between putidaredoxin and P-450$_{cam}$ is accomplished by electrostatic interactions of residues Asp34, Asp38, and Trp106 of putidaredoxin with Arg109, Arg112, and Arg79 of P-450$_{cam}$, respectively. An electron would travel from the Fe_2S_2 cluster via Cys39 and Asp38 of putidaredoxin, Arg112, and the 6-propionate of the heme to the iron center of P-450$_{cam}$ (*6*). Although the work points toward the residues involved in formation of the binary putidaredoxin−P-450 complex and proposes an electron transfer path from the Fe_2S_2 donor to the heme acceptor group, it provides no information about conformational changes in the proteins which might modulate subsequent transfer of the second electron. However, the same binding site seems to be involved in both electron transfer steps (*7*).

When the available crystallographic data of the ferric camphor−P-450$_{cam}$ complex (*8*) are compared with those of the ferrous CO-ligated camphor−P-450 structure (*9*), the main structural differences are characterized by 0.41 Å in-plane movement of the heme iron and a 140° flip of one of the heme vinyl groups; however, it is not clear whether the latter may be the result of changes in the electronic properties of the heme following reduction or is an effect of CO binding. Because the structure of the ferrous camphor−P-450 complex is not known, it is not possible to distinguish between redox transition-induced and CO ligation-

† This work was supported by grants from the Volkswagen Foundation (I/73083) and the Deutsche Forschungsgemeinschaft (Sk35/3-1).

* To whom correspondence should be addressed. Telephone: +49 30 9406 3370. Fax: +49 30 9406 3329. E-mail: cjung@mdc-berlin.de.

[1] Abbreviations: P-450$_{cam}$, cytochrome P-450 from *P. putida*; bpy, 2,2′-bipyridyl; Cat, catalase; COD, carbon monoxide difference spectrum between the carbon monoxide-ligated ferrous P-450 and the unligated ferrous P-450; EDTA, ethylenediaminetetraacetic acid disodium salt; FT, Fourier transform; GOd, glucose oxidase; IR, infrared; NHE, normal hydrogen electrode; P-420, inactive form of cytochrome P-450 with Soret band maximum absorption at 420 nm; Pdx, putidaredoxin.

10.1021/bi991759u CCC: $18.00
Published on Web 11/17/1999

induced structural changes of the protein matrix.

Several spectroscopic methods are available for probing redox transition-induced changes in cytochrome P-450. However, most of them provide only information about the spin state and ligation sphere of the heme iron (EPR and Mössbauer spectroscopy) and the electronic states and vibrational modes of the heme (UV−vis and resonance Raman spectroscopy), but no information concerning the surrounding protein matrix involved in the redox transition. Circular dichroism is sensitive to protein secondary structure, but the probed spectral region overlaps with the most commonly used reducing reagent.

To study structural changes of the protein involved in the redox transition of P-450, FTIR spectroscopy is a sensitive tool for detecting conformational changes of protein secondary structure and even individual side chains. Electrochemical reduction of myoglobin, hemoglobin, and cytochrome *c* in a special optical transparent thin electrochemical cell using gold mesh electrodes allowed the observation of redox-linked conformational changes in those proteins (*10*, *11*). For an effective electrochemical reduction of the heme proteins, and so also for P-450$_{cam}$, mediating dyes are required (*12*). This infrared spectroelectrochemical method has not been applied to cytochrome P-450s so far.

We used an alternative method to introduce electrons to the enzyme. Photoexcitable electron donors such as Safranine T, lumiflavine (*13*), proflavine, acridine (*14*, *15*), or Brilliant Alizarin Blue (*16*) have been utilized to reduce ferric cytochrome P-450$_{cam}$ in connection with a sacrificial electron donor like EDTA, to avoid electron back-transfer from the heme group to the dye. Tris(2,2′-bipyridyl)ruthenium(II) complexes [Ru(bpy)$_3$)$^{2+}$] have been widely used to study the mechanism of electron transfer in heme proteins. The excited state of Ru(bpy)$_3^{2+}$ has a low redox potential E_0(Ru^{2+}*/Ru^{3+}) of −0.86 V and a lifetime of 0.62 μs and is inert to chemical decomposition (*17*). Covalent attachment of Ru(bpy)$_3^{2+}$ derivatives to specific amino acid residues allowed probing of specific electron transfer pathways. Nakano et al. (*18*) used Ru(bpy)$_3^{2+}$ to photoreduce cytochrome P-450 1A2, and Wilker et al. (*19*) demonstrated fast electron transfer from Ru^{2+} to the heme of P-450$_{cam}$ by attaching Ru(bpy)$_3^{2+}$ via aliphatic spacers to adamantane, imidazole, or ethylbenzene that binds to the active site of P-450$_{cam}$ instead of camphor.

Recently, we have established flash photolysis techniques with time-resolved step-scan Fourier transform infrared spectroscopy as a detection method for identifying changes in secondary structure and a salt link induced by CO rebinding to ferrous P-450$_{cam}$ (*20*). In the work presented here, we present first experimental data from photoreduction of P-450$_{cam}$ by Ru(bpy)$_3^{2+}$ that clearly show that structural changes in the secondary structure and in salt links occur during the redox transition. The salt link between His355, Arg112, and the 6-propionic group of the heme is proposed to be involved in the aforementioned changes in the protein.

MATERIALS AND METHODS

Materials. Cytochrome P-450$_{cam}$ from *P. putida* was expressed in *Escherichia coli* strain TB1. Isolation and purification of the protein were carried out using previously published procedures (*21*). Cytochrome P-450$_{cam}$ with an absorption ratio A_{392}/A_{280} of 1.42 was selected for the experiments and transferred into its substrate-free form by dialysis against 50 mM Tris/HCl buffer (pH 7.4, containing 5% glycerol by volume) and subsequent gel filtration over a Sephadex G25 medium (Pharmacia) column equilibrated with the same buffer. The substrate-free protein was reconcentrated by centrifugational ultrafiltration using a Centricon 30 apparatus (Amicon) and finally dialyzed against deuterated 100 mM potassium phosphate buffer (corresponding to pH 7.0) for 24 h to ensure complete H−D exchange. This 1 mM P-450 stock solution was stored at −70 °C and used for all experiments.

Ru(bpy)$_3$Cl$_2$·6H$_2$O (Aldrich) was used without further purification. A 100 mM EDTA stock solution at pH 7.7 was prepared by dissolving EDTA and addition of sodium hydroxide pellets. For infrared spectroscopy sample preparation, aqueous stock solutions of potassium phosphate buffer, Ru(bpy)$_3$Cl$_2$, and EDTA were lyophilized and redissolved in D$_2$O. This procedure was repeated twice to ensure sufficient H−D exchange.

Photoreduction Assay. Photochemical reduction monitored by UV−vis spectroscopy was carried out in 1 cm quartz cuvettes containing 100 mM potassium phosphate buffer (pH 7.3), 10 mM EDTA, 500 μM (1*R*)-camphor, 30 μM Ru(bpy)$_3$Cl$_2$, and 3 μM P-450$_{cam}$. The cuvettes were sealed with rubber septa and bubbled with N$_2$ for 1 h to remove most of the oxygen dissolved in the buffer. However, for complete oxygen removal 44 mM glucose, 40 units/mL glucose oxidase (Merck), and catalase (Sigma) had to be added as enzymatic oxygen scavengers. A cytochrome P-450$_{cam}$ stock solution was added through the septum with a microliter syringe.

UV−vis spectra were recorded on a Shimadzu UV-2101 PC spectrometer in the range from 700 to 350 nm. Extending spectrum recording into the UV range caused slow decomposition of the ruthenium complex or the protein, so it was omitted. Photoreduction of the sample was achieved by illumination with a 100 W tungsten iodine lamp, whose output was directed onto opposite sides of the sample cuvette by means of a light pipe. Repetitive cycles of illumination and spectrum recording were performed, until reduction of the P-450 was complete or 30 min of illumination time had passed. Finally, the samples were completely reduced by addition of a few crystals of sodium dithionite, and formation of inactive cytochrome P-420 was checked by means of the carbon monoxide difference (COD) spectrum.

Samples with higher P-450 concentrations were prepared so changes in the IR spectral region could be monitored. Samples composed of deuterated stock solutions contained 100 mM deuterated potassium phosphate buffer, 10 mM EDTA, 13 mM (1*R*)-camphor or camphane from a 0.7 M stock solution using ethanol-OD as the solvent, 1 mM Ru(bpy)$_3$Cl$_2$, and 0.6 mM cytochrome P-450$_{cam}$. Glycerol-d_3 (10 vol %) was added to avoid formation of bubbles and leakage of the sample cell. Solutions were gently stirred while nitrogen was blown over their surface for 30 min to remove oxygen. Samples for the IR studies did not contain the enzymatic oxygen scavenger, because these enzymes would have spectrally interfered with the amide I′ band of cytochrome P-450$_{cam}$. The sample was filled between two calcium fluoride windows separated by a 23.4 μm Teflon spacer.

A Bruker IFS66 FTIR spectrometer equipped with a liquid nitrogen-cooled HgCdTe detector was used for recording IR

spectra. Long-wave-pass filters with cut-on wavelengths of 1.65 and 3.89 μm were placed in the IR beam before and behind the sample, respectively, to enhance the signal-to-noise ratio and to protect the spectrometer optics from scattered and reflected excitation laser light. The sample was illuminated at 532 nm with light from a frequency-doubled, pulsed Nd:YAG laser (Surelite I, Continuum) running at a 10 Hz repetition rate. The energy of the excitation beam was attenuated by neutral density filters to yield 4.5 mJ of output energy per pulse on the sample.

Infrared spectra were recorded before and after illumination of the sample. Illumination intervals of 10 s (100 laser shots) were accumulated, and then spectrum recording was initiated. This cycle was repeated until no further absorption changes in the sample could be detected. For each spectrum, 512 double-sided interferometer scans were averaged, and Fourier transformed using Blackman−Harris three-term apodization and Mertz phase correction to obtain single channel intensity spectra. Absorption difference spectra were calculated from the intensity spectra $I(t)$ recorded after illumination time t and the single-channel spectrum of the oxidized sample I_{ox} as $\Delta A(t) = -\log[I(t)/I_{ox}]$. A water vapor absorption spectrum was subtracted from each difference spectrum to compensate for residual water vapor present in the sample compartment of the spectrometer.

Infrared spectra of all single components of the redox reaction mixture, as well as for the mixture without P-450, have been recorded with and without illumination to test a possible interference with signals arising from the P-450 reduction.

RESULTS

We used tris(2,2′-bipyridyl)ruthenium(II) for photochemical reduction of cytochrome P-450$_{cam}$ according to the following reaction scheme.

$$Ru(bpy_3)^{2+} \xrightarrow{h\nu} Ru(bpy_3)^{2+}* \quad (1)$$

$$Ru(bpy_3)^{2+}* + Fe^{3+} \rightarrow Ru(bpy_3)^{3+} + Fe^{2+} \quad (2)$$

$$Ru(bpy_3)^{3+} + D \rightarrow Ru(bpy_3)^{2+} + D^{+} \quad (3)$$

$$Fe^{2+} + CO \rightarrow Fe^{2+}{-}CO \quad (4)$$

$Ru(bpy)_3^{2+}$ has a charge transfer band at 452 nm ($\epsilon = 14\,600$ M^{-1} cm^{-1}). The long-lived excited state of $Ru(bpy)_3^{2+}*$ (eq 1) with a luminescence lifetime of 0.62 μs can act as a strong reducing reagent [$E_0(Ru^{2+}*/Ru^{3+}) = -0.86$ V vs NHE] (*17*). Electrons flow from $Ru(bpy)_3^{2+}*$ to the ferric heme group of cytochrome P-450$_{cam}$. $E_0(Fe^{3+}/Fe^{2+})$ is −170 mV for camphor-bound P-450$_{cam}$ and −303 mV for substrate-free P-450$_{cam}$ (*22*).

To avoid back electron transfer from the ferrous heme to $Ru(bpy)_3^{3+}$, EDTA serves as the sacrificial electron donor D to reduce $Ru(bpy)_3^{3+}$ (eq 3). To protect the ferrous heme from autoxidation due to traces of oxygen, it can be trapped by formation of the stable heme−carbon monoxide complex (eq 4).

The UV−visible spectra of illuminated substrate-free cytochrome P-450$_{cam}$ in the presence of $Ru(bpy)_3^{2+}$ and EDTA exhibit a decrease in the intensity of the Soret band at 417 nm together with a small shift to 416 nm (Figure 1A) compared to the spectrum before illumination. Simultaneously, the Q-bands at 569 and 536 nm increase and become less separated at 558 and 538 nm. These spectral shifts are in agreement with the transition from the ferric low-spin to the ferrous high-spin state of the heme iron. However, there is only partial reduction of cytochrome P-450$_{cam}$. On complete reduction by addition of excess sodium dithionite, the Soret band shifted to 410 nm, and the Q-band position was found at 541 nm. The difference spectra of the illuminated-minus-ferric P-450 recorded at various illumination times (inset of Figure 1A) is dominated by an intense minimum at 418 nm. A corresponding increase of a positive band is not observed because of spectral compensation effects due to the broad spectrum of the reduced complex. Isosbestic

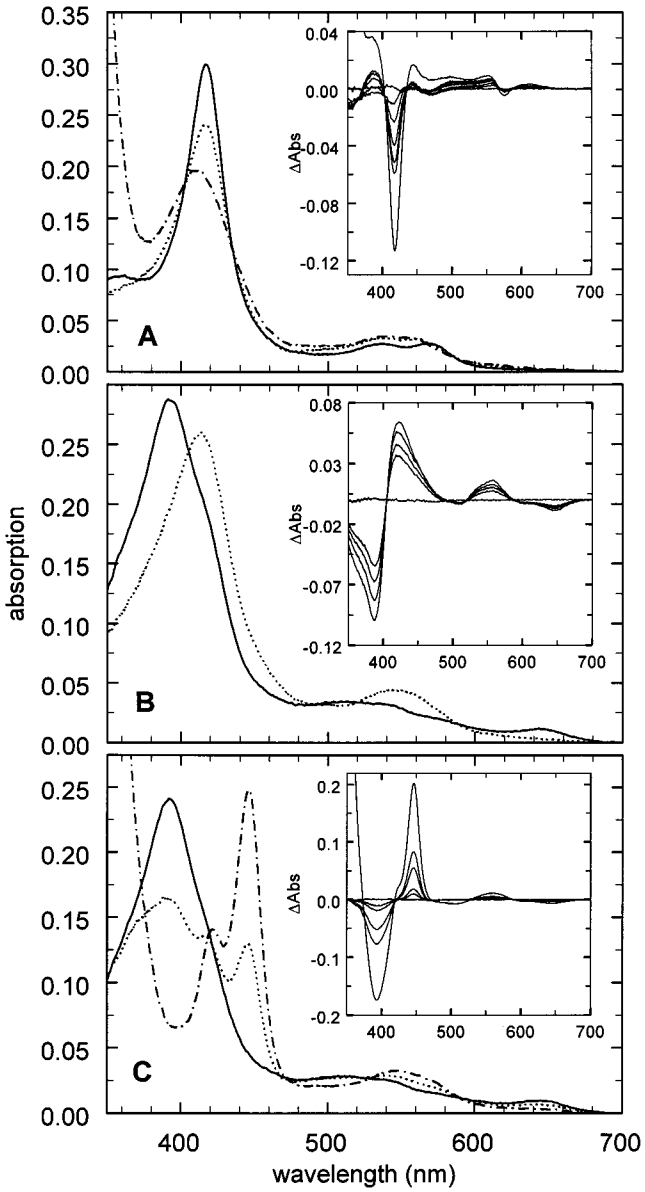

FIGURE 1: UV−visible spectra of oxidized (solid line), photoreduced (dotted line), and dithionite-reduced (dashed line) cytochrome P-450$_{cam}$ in 100 mM phosphate buffer (pH 7.3), 10 mM EDTA, 44 mM glucose, 30 μM $Ru(bpy)_3Cl_2$, 40 units/mL glucose oxidase, and catalase measured in 1 cm quartz cuvettes: (A) substrate-free P-450$_{cam}$, (B) camphor-bound P-450$_{cam}$, and (C) camphor-bound P-450$_{cam}$ in carbon monoxide-saturated buffer. Spectra were corrected by subtraction of glucose oxidase and $Ru(bpy)_3Cl_2$ spectra. The insets show differences between spectra taken at increasing illumination times minus spectra of the oxidized P-450.

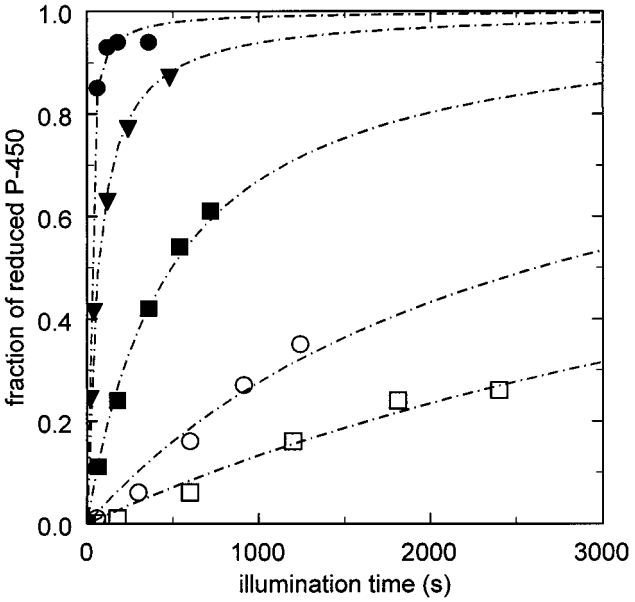

FIGURE 2: Effect of substrate binding and GOd/Cat on the reduction efficiency of P-450: (●) camphor−P-450$_{cam}$ with GOd/Cat, (▼) camphane−P-450$_{cam}$ with GOd/Cat, (■) substrate-free P-450$_{cam}$ with GOd/Cat, (○) N_2-purged camphor−P-450$_{cam}$, and (□) substrate-free N_2-purged P-450$_{cam}$.

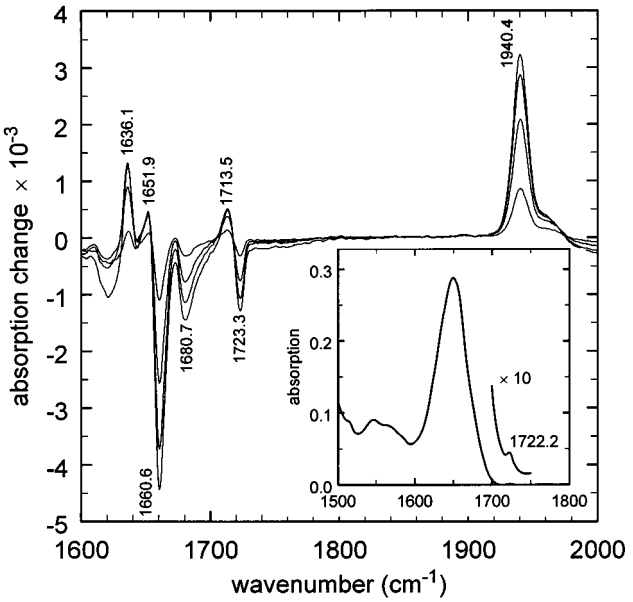

FIGURE 3: Infrared difference spectrum of the reduced CO complex-minus-oxidized P-450$_{cam}$ taken after illumination for 20, 60, 130, and 340 s. The inset shows the infrared absorption spectrum of oxidized cytochrome P-450$_{cam}$ in D_2O in its substrate-bound form. The large amide I′ band at 1650 cm^{-1} has a small sideband at 1722 cm^{-1} (10-fold enlarged) from the C═O stretch vibration of COOD groups. The sample contained 0.54 mM P-450 in 100 mM phosphate buffer, 1 mM Ru(bpy)$_3^{2+}$, 10 mM EDTA, 10 mM camphor, and 10% glycerol-d_3. The same buffer containing Ru(bpy)$_3^{2+}$, EDTA, and camphor at identical concentrations was used as a reference to calculate the absorption spectrum.

points at 403, 437, 566, and 589 nm give rise to the assumption that only two well-defined states are involved in the process. When the difference spectra obtained from illumination are compared to dithionite-reduced difference spectra, the shape of the spectra proves that the observed spectral changes arise from reduction of cytochrome P-450$_{cam}$.

On illumination of camphor-bound P-450$_{cam}$ (Figure 1B), the Soret band shifts from 392 to 414 nm, the characteristic high-spin state band at 646 nm vanishes, and the Q-band for the reduced P-450 at 544 nm appears. Spectral changes were completed within 2 min of illumination under anaerobic conditions as described in Materials and Methods, and no further reduction by addition of dithionite was observed. Difference spectra between illuminated P-450 samples and a dark reference sample (inset of Figure 1B) recorded after various illumination times exhibit a characteristic S shape with a maximum at 422 nm and a minimum at 388 nm. Isosbestic points are at 405, 491, 521, and 589 nm.

Illumination of camphor-bound P-450 was repeated in a buffer saturated with carbon monoxide and produces a shift of the Soret band from 392 to 446 nm (Figure 1C). Because carbon monoxide binds only to the ferrous form of P-450, the observation of the characteristic Soret band at 446 nm gives additional evidence of the ferric-to-ferrous transition of the heme iron. However, a small shoulder at 416 nm in the photoreduced spectrum, which shifts to 421 nm after complete reduction due to addition of dithionite, arises from the formation of a small amount of P-420, the inactive form of P-450.

To quantify the efficiency of the photoreduction of cytochrome P-450, the illumination dose required for reducing 50% of the initial P-450 concentration was determined from a plot of the fraction of reduced P-450, $f_{red}(t)$, versus illumination time t (Figure 2) by fitting to the function $f_{red}(t) = (t/t_{1/2} + t)$, where $t_{1/2}$ is the time required to reduce 50% of the protein (half-reduction time) and $f_{red}(t)$ was determined from the fraction of the maximum absorption change after exposing the sample for a given illumination time to the maximum absorption change obtained from dithionite reduction. When half-reduction times of substrate-free versus camphor-bound P-450 are compared (Table 1), the reduction efficiency of substrate-free P-450 is decreased by a factor of 41. Samples prepared without the enzymatic oxygen scavenger system GOd/Cat exhibit a drastically lower reduction efficiency compared to those samples containing the oxygen scavenger; the reduction efficiency of camphor-bound P-450 decreases by a factor of 239 and that of substrate-free P-450 by a factor of 14.6. Oxygen acts as an efficient quencher to the excited state of Ru(bpy)$_3^{2+}$* by an energy transfer quenching mechanism with a quenching rate k_q of 3.3×10^9 M^{-1} s^{-1} (*17*), and it can reoxidize the ferrous P-450 via the autoxidation path ($k_a = 0.015$ s^{-1} at 22 °C) by formation of O_2^- superoxide anions (*23*). Both quenching paths will give a lower yield of ferrous P-450.

Additional tests were made to check the influence of glucose oxidase and catalase on the photoreduction, because GOd contains a flavine group which could also act principally as an electron donor for photoreduction (*24*). In samples containing no Ru(bpy)$_3$Cl$_2$, reduction of P-450$_{cam}$ was also observed when GOd/Cat was present at identical half-reduction times as determined for samples containing Ru(bpy)$_3$Cl$_2$. This observation leads to the preliminary conclusion that GOd is also a competent electron donor to P-450$_{cam}$.

No reduction of cytochrome P-450$_{cam}$ was observed in absence of EDTA as a sacrificial electron donor to Ru(bpy)$_3^{2+}$.

The inset of Figure 3 shows the IR absorption spectrum of oxidized camphor-bound P-450$_{cam}$ in the amide I′ region

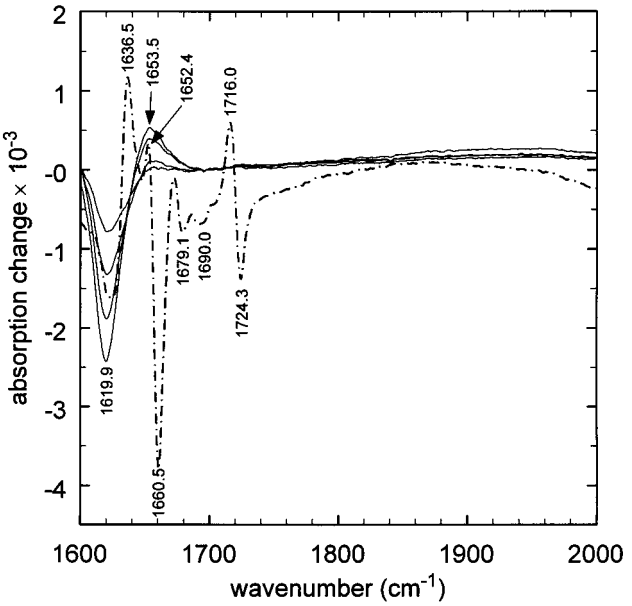

FIGURE 4: Control experiment demonstrating the effect of EDTA. Phosphate buffer (100 mM) containing 10 mM EDTA, 1 mM Ru(bpy)$_3^{2+}$, 10 mM camphor, and 10% glycerol-d_3 was illuminated for 60, 120, 180, and 240 s. The dashed line shows the reduced-minus-oxidized difference spectrum of camphor-bound P-450$_{cam}$.

Table 1: Half-Illumination Time $t_{1/2}$ Obtained from Fitting the Data Depicted in Figure 2 to the Function $f_{red}(t) = t/(t_{1/2} + t)$

sample	$t_{1/2}$ (s) with GOd/Cat	$t_{1/2}$ (s) without God/Cat	E_0' (mV)
substrate-free P-450	450	6579	−303
camphor-bound P-450	11	2629	−170
camphane-bound P-450	65	nd	−183[a]

[a] Estimated from the relation between E_0' and high-spin content (*22*).

in deuterated buffer. The main band centered at 1646 cm^{-1} arises from C═O stretch vibrations of the protein backbone and resembles multiple sub-bands which can be assigned to individual protein secondary structure elements (*26*, *27*). There is also a small sideband centered at 1722 cm^{-1} which can be assigned to C═O stretch vibrations of COOD groups. The same small sideband is also seen in the camphane complex, but not in substrate-free P-450$_{cam}$. Other compounds present in the reduction assay absorb at 1606.1 [Ru(bpy)$_3$Cl$_2$], 1583.9, and 1623.3 cm^{-1} (deprotonated and protonated forms of EDTA, respectively), and thus can be excluded to contribute to the 1722 cm^{-1} signal. The photoreduced-minus-oxidized difference spectra (Figures 3 and 5B) recorded at increasing illumination times exhibit significant changes in the amide I′ region between 1610 and 1690 cm^{-1} which are summarized in Table 2. These bands are due to C═O stretch vibrations that couple to N−D bending and C−N stretching modes. In analogy to the assignment of amide I′ bands to secondary structure elements made for other proteins (*28*) and for cytochrome P-450$_{cam}$ (*29*), the positive peak at 1636.1 cm^{-1} can be assigned to an increasing 3_{10}-helical or β-sheet content, and the negative peaks at 1660.6 and 1680.7 cm^{-1} are assigned to decreasing α-helical and turn structure content, respectively. The negative peak at 1621.0 cm^{-1} is in a region where β-sheets are expected. However, control experiments in the absence of protein showed that this signal is dominated by an EDTA signal, induced by interaction of

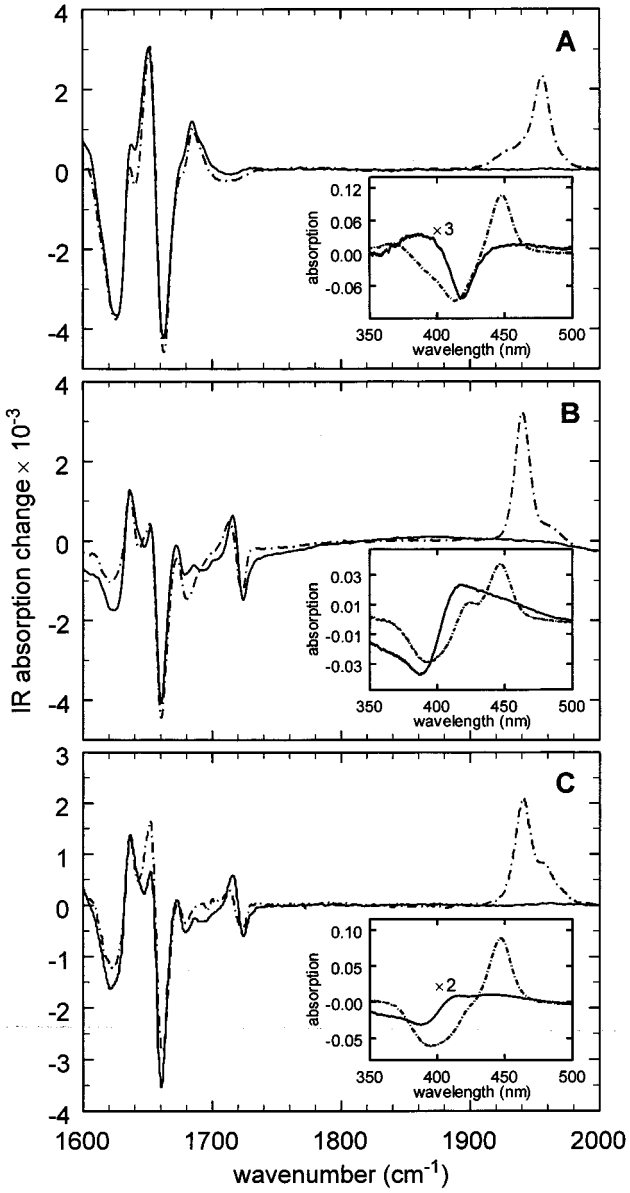

FIGURE 5: Infrared absorption difference spectra of photoreduced-minus-oxidized P-450$_{cam}$ (solid line) and photoreduced CO-bound-minus-oxidized P-450$_{cam}$ (dashed line). The insets show the UV−vis difference spectra of reduced-minus-oxidized (solid line) and of reduced CO-bound-minus-oxidized P-450$_{cam}$ (dashed line) measured in 23.4 μm IR sample cells. Samples were composed of 0.6 mM P-450 in 100 mM deuterated phosphate buffer, 1 mM Ru(bpy)$_3$Cl$_2$, 10 mM EDTA, and 10% (by volume) glycerol-d_3: (A) substrate-free P-450, (B) camphor−P-450, and (C) camphane−P-450. The substrate concentration was 13 mM for panels B and C. For the CO-bound spectra, the buffer was saturated with CO prior to loading of the IR sample cell.

EDTA with the CaF_2 window material of the IR sample cell (Figure 4). The positive peak at 1713.5 cm^{-1} and the negative peak at 1723.3 cm^{-1} are assigned to the C═O stretch vibration of a COOD group from aspartic acid, glutamic acid, or heme propionate side chain residues. The nearly symmetric S shape of the two bands suggests a shift of the C═O stretch band in the absolute absorption spectrum (Figure 3 inset) which could be due to a lengthening of a C═O···D hydrogen bond within the COOD group. However, the assignment of a COOD group is still ambiguous, because the camphor keto group has a band at nearly the same position (1716 cm^{-1}). The intense band at 1940 cm^{-1} originates from the C═O

Table 2: Signals Observed in Infrared Difference Spectra (photoreduced-minus-oxidized)[a]

ν (cm^{-1})						
(1*R*)-camphor without CO	(1*R*)-camphor with CO	camphane without CO	camphane with CO	substrate-free without CO	substrate-free with CO	tentative assignment
	1940.4 (+)		1941.0 (+)		1955.8 (+)	ν_{str} heme iron C═O
1724.3 (−)	1723.3 (−)	1723.3 (−)	1723.0 (−)			heme 6-propionic group salt-linked
1716.0 (−)	1713.5 (−)	1716.0 (+)	1713.1 (+)			to His355 and Arg112
				1714.8 (−)	1708.8 (−)	broad weak band
1690.0 (−)		1692.5 (−)	1696.1 (−)			turns
1679.1 (−)	1680.7 (−)	1679.4 (−)	1679.2 (−)	1684.9 (−)	1685.2 (−)	turns
				1662.5 (−)	1662.2 (−)	turns or α-helix
1660.5 (−)	1660.6 (−)	1660.6 (−)	1661.3 (−)			α-helix
1652.4 (+)	1651.9 (+)	1652.2 (+)	1652.1 (+)	1651.3 (+)	1652.2 (+)	α-helix
1636.5 (+)	1636.1 (+)	1636.6 (+)	1636.5 (+)		1636.7 (+)	3_{10}- or α-helix

[a] (+) and (−) correspond to positive and negative bands and to increasing and decreasing amounts of structure change due to reduction, respectively.

stretch vibration of heme iron-bound CO (*21*) and proves that the heme iron is reduced also under the higher-protein concentration conditions necessary for IR spectroscopy. A small shoulder at 1960 cm^{-1} indicates formation of some P-420 during photoreduction.

In the absence of carbon monoxide, small differences for the carbon monoxide-bound P-450 can be seen in Figure 5B, a decrease in the level of turn structures, which splits into two small negative bands located at 1690.0 and 1679.1 cm^{-1} (Table 2).

Replacing the natural substrate (1*R*)-camphor with camphane, which lacks the camphor keto group, has no effect on the position of the 1722 cm^{-1} band in the absolute absorption spectrum (inset of Figure 3). Changes in the amide I′ band due to photoreduction (Figure 5C) are almost identical to those of (1*R*)-camphor-bound P-450_{cam}. Band positions of the reduced-minus-oxidized absorption difference spectra of camphane-bound and camphor-bound P-450_{cam} are identical within the measurement resolution of 2 cm^{-1} (Table 2). Additional CO binding to camphane−P-450_{cam} (Figure 5C) causes an increase in the magnitude of the 1652.1 cm^{-1} peak from α-helical structure. The signals at 1724.3 and 1716.0 cm^{-1} are unaffected by the absence of a substrate keto group, so they can be assigned to originate from changes in protein salt links and not from hydrogen bonds to a substrate keto group.

In contrast to camphor- or camphane-bound P-450_{cam}, the substrate-free protein difference spectra show distinct differences (Figure 5A). In the reduced-minus-oxidized difference spectrum (Table 2), the 1724 and 1716 cm^{-1} peak pair is missing, and instead, there is a weak broad negative band with a minimum at 1714.8 cm^{-1}. A positive peak at 1684.9 cm^{-1} indicates an increasing level of turns. The assignment of the 1662.5 cm^{-1} signal to either turns or α-helices is equivocal, but the positive peak at 1651.3 cm^{-1} might indicate an increasing level of α-helical structure. CO binding to the reduced substrate-free P-450_{cam} gives rise to a shift of the weak band from 1714.8 to 1708.8 cm^{-1}, a narrowing of the turn signal at 1685.2 cm^{-1}, and a decreasing amplitude of the 1636.7 cm^{-1} peak from β-sheets or 3_{10}-helices. The C═O stretch vibration of the heme-bound CO has a maximum at 1955.8 cm^{-1} and a minor band between 1930 and 1940 cm^{-1} which corresponds to the multiple CO stretch modes of substrate-free P-450_{cam} observed previously (*30*).

Samples for IR spectroscopy had to be prepared with an approximately 200-fold higher protein concentration, and the concentration ratio of P-450 to $Ru(bpy)_3^{2+}$ was lowered to 2, compared to 10 for the photoreduction experiments whose results are shown in Figure 1. Despite these drastically changed conditions, UV−vis absorption spectra of oxidized P-450_{cam} and of illuminated samples measured directly in the IR sample cell indicate formation of reduced and reduced CO-bound P-450_{cam}, respectively, independently from the IR spectra, for substrate-free, camphor-bound, and camphane-bound enzymes; reduced-minus-oxidized difference spectra of substrate-free and camphor-bound P-450 (insets of panels A and B of Figure 5) are identical to those in panels A and B of Figure 1. Camphane-bound oxidized P-450_{cam} (inset of Figure 5C) contains 86% of the high-spin heme, as determined using the fit procedure described previously (*25*). As a consequence, the difference spectrum of camphane-bound P-450 shown in the inset of Figure 5C is a linear combination of the high-spin difference spectrum (ΔA_{HS}, inset of Figure 5B) and the low-spin difference spectrum (ΔA_{LS}, inset of Figure 5A), and a similiar value (78%) is found when fitting the spectrum to the linear equation $\Delta A_{camphane} = x\Delta A_{HS} + (1 - x)\Delta A_{LS}$, with x being the fraction of high-spin P-450.

If illumination of P-450_{cam} was performed in carbon monoxide-saturated buffer, formation of the heme−carbon monoxide complex was observed, as indicated by the characteristic 447 nm Soret band (insets of Figure 5).

To differentiate between the structural changes induced by reduction and by carbon monoxide binding, we calculated the Fe^{2+}-minus-(Fe^{2+}−CO) difference spectrum by subtracting the Fe^{2+}-minus-Fe^{3+} spectrum from the (Fe^{2+}−CO)-minus-Fe^{3+} difference spectrum of Figure 5B for the camphor−P-450_{cam} complex. When this spectrum is compared to the transient light-minus-dark difference spectrum obtained from flash photolysis experiments with the ternary camphor−carbon monoxide−P-450 complex (*20*), good agreement between the static Fe^{2+}-minus-(Fe^{2+}−CO) difference spectrum measured by photoreduction with $Ru(bpy)_3^{2+}$ and time-resolved FTIR Fe^{2+}-minus-(Fe^{2+}−CO) difference spectrum could be observed (Figure 6 and Table 3). Only at 1676 cm^{-1} is a difference between both spectra seen, which might originate from the small amount of P-420 generated during the experiments, as can be seen from the UV−vis spectrum (Figure 5B) and a minor band at 1960 cm^{-1} in the IR difference spectra (Figures 5B and 6).

Trying the same comparison for the substrate-free protein is discouraging because of the high noise level of flash photolysis data recently determined (*20*) in the amide I′

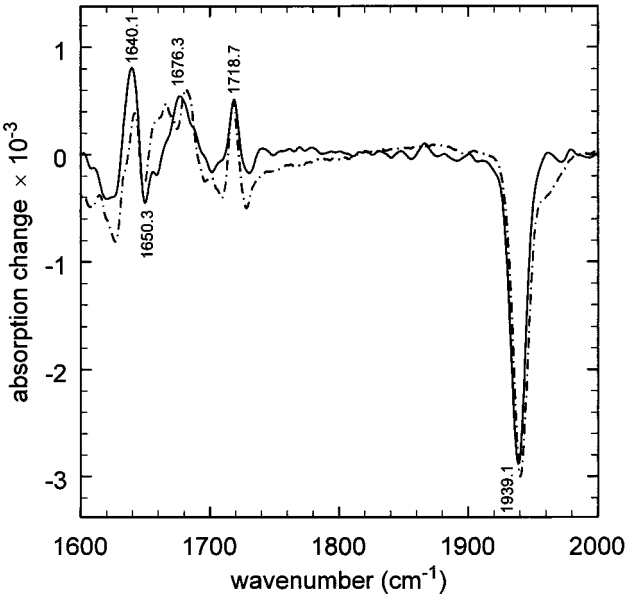

FIGURE 6: Comparison of the effect of CO binding on the secondary structure of camphor-bound P-450$_{cam}$. Both spectra are the difference of the reduced-minus-reduced CO-bound state. The solid line represents the transient absorption difference recorded 40 μs after applying a nanosecond laser flash to reduced CO-bound camphor−P-450$_{cam}$ from flash photolysis experimtents (*20*). The dashed line represents the difference between the two spectra shown in Figure 5B. For better comparison, the transient flash photolysis spectrum was scaled to equal the CO stretch band area of the spectrum obtained from photoreduction.

Table 3: Signals of Camphor-Bound P-450−CO-Minus-Reduced P-450 Difference Spectra Calculated from Photoreduction and Observed in Flash Photolysis Experiments (*20*)

ν (cm^{-1})		
photoreduction	flash photolysis	tentative assignment
1940.8 (−)	1939.1 (−)	ν_{str} heme iron C═O
1719.0 (+)	1718.7 (+)	salt link between the heme 7-propionic group and Arg299
1676.3 (+)	1676.3 (+)	turns
1651.4 (−)	1650.3 (−)	α-helix
1641.8 (+)	1640.1 (+)	3_{10}- or α-helix

bands. In addition, it should be noted that the transient C═O stretch vibration of substrate-free P-450$_{cam}$ has its main band at 1940 cm^{-1}, while the main band in the CO-bound reduced-minus-oxidized difference spectrum is located at 1955 cm^{-1}. This is possibly an effect of different CO rebinding rates obeyed by the taxonomic substates of the C═O stretch mode.

DISCUSSION

Photoreduction of P-450$_{cam}$. From the spectroscopic data, it should be evident that P-450$_{cam}$ is photoreduced by Ru(bpy)$_3^{2+}$. However, compared to that by other electron donors such as Safranine T, reduction by Ru(bpy)$_3^{2+}$ proceeds rather slowly and the question is why? Compared to Safranine T, the excited state of Ru(bpy)$_3^{2+}$ has a much lower redox potential [E_0(Ru^{2+}*/Ru^{3+}) = −0.86 V vs NHE] (*17*), so one would expect a fast reduction. However, it is known that electron transfer to P-450 is a slow process; it is the rate-limiting step for substrate turnover, so quenching of the Ru^{2+}* excited state and autoxidation of P-450 by oxygen traces become more important. There are possibly unfavorable electrostatic boundary conditions for the electron transfer. The best position on the surface of P-450$_{cam}$ for electron transfer is the *P. putida* redoxin binding site. This binding site is partially positively charged, and putidaredoxin carries a partially negative countercharge. Unfortunately, Ru(bpy)$_3^{2+}$ has a positive charge, so it will temporarily bind somewhere on the protein surface but not into the favorable Pdx binding site, with the disadvantage of a much longer spatial distance between the redox centers.

Infrared Spectroscopy of P-450$_{cam}$. From the absorption difference spectra, it can be seen that not only the heme but also the whole protein secondary structure is affected by the redox transition. For substrate-bound P-450, turn content seems to decrease, while 3_{10}- or α-helix contents increase. Potential changes in the β-structure are masked in the IR spectra by a signal from EDTA interaction with the CaF_2 window material. The simultaneous increase in the magnitude of α-helix signals at 1652 cm^{-1} and the decrease at 1660 cm^{-1} could result either from different α-helices affected by the redox transition or from an α−α transition of one helix; unambiguous differentiation between the two mechanisms is not possible. The same effect is seen in substrate-free P-450 for the turn signals at 1685 (+) and 1662 cm^{-1} (−). It has not yet been possible to assign the signals to individual residues, which would be necessary for a deeper understanding. When the overall effects of redox transition and CO ligand binding are compared, the redox transition involves many more changes in the protein secondary structure than CO binding as can be concluded from the amplitude of the absorbance difference seen in flash photolysis spectra.

Assignment of the 1716 and 1724 cm^{-1} Peaks. Infrared absorption around 1720 cm^{-1} is normally from the C═O stretch vibration of carboxylic acid groups of glutamic acid, aspartic acid, or the propionic groups of the heme. Keto groups in five- and six-membered cyclic aliphatic compounds can also absorb in the same range, especially (1*R*)-camphor which has a signal at 1716 cm^{-1} in aqueous solution that shifts to 1736 cm^{-1} with $CHCl_3$ as the solvent. However, replacing (1*R*)-camphor with camphane, which lacks the keto group, has no effect on the reduced-minus-oxidized difference spectrum, or on the peak at 1722 cm^{-1} in the absolute spectrum. Therefore, it can be ruled out that a change in hydrogen bonding of the substrate due to the redox transition is the origin of these signals. The C═O stretch vibration of the free amino acids of aspartic acid and glutamic acid at pD 1.4 is observed at 1713 cm^{-1} for aspartic acid (C_βOOD) and at 1706 cm^{-1} for glutamic acid (C_γOOD). The side chains of other amino acids have no signal in this spectral region (*31*). Similarly, the propionic acid groups of protoporphyrin IX exhibit infrared bands at 1740 cm^{-1} (*32*) that can be modulated by hydrogen bonding to arginine, lysine, or histidine residues in the range from 1740 to 1700 cm^{-1}. This has been extensively studied for bacteriorhodopsin (*33*), and is also known for cytochromes *c* (*10*). So we assign these signals to a salt link. Electrostatic free energy calculations for ionic pairs in the cytochrome P-450$_{cam}$ structure brought to light 32 salt links that stabilize the protein's folded state (*34*). Excluding all salt links which are too distant from the heme to be affected by the redox transition, the heme propionic groups remain the best candidates (Figure 7). The 6-propionic group is involved in a salt link between Arg112

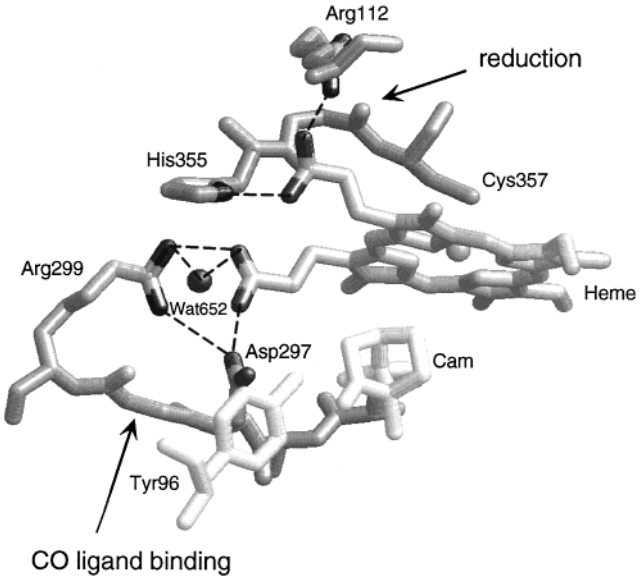

FIGURE 7: Active site of P-450$_{cam}$ and amino acid residues proposed to be involved in the salt links affected by redox transition and carbon monoxide binding. Atom coordinates were taken from oxidized camphor-bound P-450$_{cam}$ (*8*), PDB file 2CPP.

and His355, while the 7-propionic group forms a salt link with Arg299 and Asp297. The latter has been shown to be involved in CO rebinding from flash photolysis experiments (*20*), while the first was proposed to be involved in electron transfer from putidaredoxin to P-450$_{cam}$ (*6*).

ACKNOWLEDGMENT

We are grateful to Udo Heinemann for carefully reading the manuscript and for critical comments.

REFERENCES

1. Schenkmann, J. B., and Greim, H. (1993) in *Handbook of Experimental Pharmacology*, Vol. 105, Springer-Verlag, Berlin.
2. Guengerich, F. P. (1991) *J. Biol. Chem. 266*, 10019−10022.
3. Porter, T. D., and Coon, M. J. (1991) *J. Biol. Chem. 266*, 13469−13472.
4. Sligar, S. G., and Murray, R. I. (1986) in *Cytochrome P-450: Structure, Mechanism, and Biochemistry* (Ortiz de Montellano, P. R., Ed., pp 429−503, Plenum Press, New York.
5. Mueller, E. J., Loida, P. J., and Sligar, S. G. (1996) in *Cytochrome P450: Structure, Mechanism, and Biochemistry* (Ortiz de Montellano, P. R., Ed.) 2nd ed., pp 83−124, Plenum Press, New York.
6. Roitberg, A. E., Holden, M. J., Mayhew, M. P., Kurnikov, I. V., Beratan, D. N., and Vilker, V. L. (1998) *J. Am. Chem. Soc. 120*, 8927−8932.
7. Unno, M., Shimada, H., Toba, Y., Makino, R., and Ishimura, Y. (1996) *J. Biol. Chem. 271*, 17869−17874.
8. Poulos, T. L., Finzel, B. C., and Howard, A. J. (1987) *J. Mol. Biol. 195*, 687−700.
9. Raag, R., and Poulos, T. L. (1989) *Biochemistry 28*, 7586−7592.
10. Moss, D., Nabedryk, E., Breton, J., and Mäntele, W. (1990) *Eur. J. Biochem. 187*, 565−572.
11. Schlereth, D. D., and Mäntele, W. (1992) *Biochemistry 31*, 7494−7502.
12. Huang, Y.-Y., Hara, T., Sligar, S. G., Coon, M. J., and Kimura, T. (1986) *Biochemistry 25*, 1390−1394.
13. Hintz, M. J., and Peterson, J. A. (1980) *J. Biol. Chem. 255*, 7317−7325.
14. Tyson, C. A., Lipscomp, J. D., and Gunsalus, I. C. (1972) *J. Biol. Chem. 247*, 5777−5784.
15. Greenbaum, E., Austin, R. H., Frauenfelder, H., and Gunsalus, I. C. (1972) *Proc. Natl. Acad. Sci. U.S.A. 69*, 1273−1276.
16. Sligar, S. G., and Gunsalus, I. C. (1976) *Proc. Natl. Acad. Sci. U.S.A. 73*, 1078−1082.
17. Kalyanasundaram, K. (1982) *Coord. Chem. Rev. 46*, 159−244.
18. Nakano, R., Hideaki, S., and Shimizu, T. (1996) *J. Photochem. Photobiol., B 32*, 171−176.
19. Wilker, J. J., Dmochowski, I. J., Dawson, J. H., Winkler, J. R., and Gray, H. B. (1999) *Angew. Chem. 111*, 94−96.
20. Contzen, J., and Jung, C. (1998) *Biochemistry 37*, 4317−4324.
21. Jung, C., Hui Bon Hoa, G., Schröder, K.-L., Simon, M., and Doucet, J. P. (1992) *Biochemistry 31*, 12855−12862.
22. Fisher, M. T., and Sligar, S. G. (1985) *J. Am. Chem. Soc. 107*, 5018−5019.
23. Sligar, S. G., Lipscomp, J. D., Debrunner, P. G., and Gunsalus I. C. (1974) *Biochem. Biophys. Res. Commun. 61*, 290−296.
24. Hecht, H. J., Kalisz, H. M., Hendle, J., Schmid, R. D., and Schomburg, D. (1993) *J. Mol. Biol. 229*, 153−172.
25. Jung, C., Ristau, O., and Rein, H. (1991) *Biochim. Biophys. Acta 1076*, 130−136.
26. Byler, D. M., and Susi, H. (1986) *Biopolymers 25*, 469−487.
27. Susi, H., and Byler, D. M. (1986) *Methods Enzymol. 130*, 290−311.
28. Krimm, S., and Bandekar, J. (1986) *Adv. Protein Chem. 38*, 181−364.
29. Mouro, C., Jung, C., Bondon, A., and Simonneaux, G. (1997) *Biochemistry 36*, 8125−8134.
30. Jung, C., Ristau, O., Schulze, H., and Sligar, S. G. (1996) *Eur. J. Biochem. 235*, 660−669.
31. Chirgadze, Y. N., Fedorov, O. V., and Trushina, N. P. (1975) *Biopolymers 14*, 679−694.
32. Spiro, T. G (1983) in *Physical Bioinorganic Chemistry Series: Iron Porphyrins, Part III* (Lever, A. B. P., and Gray, H. B., Eds.) pp 89−159, Addison-Wesley, London.
33. Bousché, O., Sonar, S., Krebs, M. P., Khorana, H. G., and Rothschild, K. J. (1992) *Photochem. Photobiol. 56*, 1085−1095.
34. Lounnas, V., and Wade, R. C. (1997) *Biochemistry 36*, 5402−5417.

BI991759U